Research Article | Vol. 32, No. 15 / 15 Jul 2024 / Optics Express 25892

Optics EXPRESS

Two-color 3D printing for reduction in femtosecond laser printing power

ANWARUL ISLAM AKASH, JASON E. JOHNSON, FREDRIK C. ARENTZ, AND XIANFAN XU*

School of Mechanical Engineering and Birck Nanotechnology Center, Purdue University, 1205 Mitch Daniels Blvd., West Lafayette, IN 47907, USA
**xxu@ecn.purdue.edu*

Abstract: Two-photon polymerization (TPP) has emerged as a favored advanced manufacturing tool for creating complex 3D structures in the sub-micron regime. However, the widescale implementation of this technique is limited partly due to the cost of a high-power femtosecond laser. In this work, a method is proposed to reduce the femtosecond laser 3D printing power by as much as 50% using a combination of two-photon absorption from an 800 nm femtosecond laser and single photon absorption from a 532 nm nanosecond laser. The underlying photochemical process is explained with modeling of the photopolymerization reaction. The results show that incorporating single-photon absorption from a visible wavelength laser efficiently reduces inhibitor concentration, resulting in a decreased requirement for femtosecond laser power. The radical to macroradical conversion is dominated by the reduction in oxygen concentration, while the reduction in photoinitiator concentration limits the threshold power reduction of the femtosecond laser.

1. Introduction

Two-photon lithography (TPL) pioneered by Maruo et al. [1,2] can print features beyond the traditional diffraction limit of light, exploiting the nonlinearity arising from two-photon absorption [3–5]. To further improve the resolution and feature size, several techniques including Stimulated Emission Depletion (STED) [6,7] and STED-inspired multi-color photolithography [8–16] have been implemented to optically inhibit polymerization only in the periphery of the laser spot, resulting in printed linewidths within 9-30 nm range. The use of two beams may also lead to the reduction of power of the femtosecond laser pulse [16]. Additionally, the relatively slow point-by-point laser scanning of two-photon direct-laser-writing (DLW) can be scaled up utilizing techniques like multi-foci scanning [17,18], projection lithography [19,20] and digital holography based TPL [21,22]. The superiority in resolution and speed led to TPL being used to create nanostructures for applications in micro-optics [23,24], photonics [25], biomedical devices [26], emerging materials [27], and so on. However, the widespread application beyond the microscale is still limited, partly due to the cost of a high-power femtosecond (fs) laser that is fundamental to achieving nonlinearity in the absorption process.

Efforts have been made to reduce the cost associated with the 3D printing process by using (1 + 1)-photon absorption methods [28–30]. These methods seek to imitate the nonlinearity of TPL without requiring a fs laser. Instead, they replace the virtual intermediate state in TPL with a real intermediate electronic state in a single photon absorption pathway [28], use triplet-triplet annihilation [29], or triplet fusion upconversion [30]. However, they still suffer from residual single-photon absorption (1PA) effects. In this work, we propose a method to reduce the power requirement of the fs laser itself by combining the effects of two-photon absorption (TPA) and 1PA simultaneously. Our method differs from typical two-color lithography methods in that both lasers contribute to the excitation process, rather than one laser exciting the molecule and

#525826 https://doi.org/10.1364/OE.525826
Journal © 2024 Received 8 Apr 2024; revised 24 May 2024; accepted 29 May 2024; published 2 Jul 2024

Optics EXPRESS

the other inhibiting the excitation process. As TPA still dominates this process, the resolution superiority inherent to typical TPL can be maintained.

To better understand the photochemical processes and gain further insights from experimental findings, it is necessary to develop a mathematical model for the two-color printing process. Numerous models have been developed over the years to understand 3D nanolithography by two-photon polymerization, including the polymerization kinetics [31–37] and the excited state kinetics [28,38]. Our previous work presented a comprehensive photopolymerization model considering both the excited state and subsequent polymerization kinetics [39]. Here we extend this model to compute the combined effect of TPA and 1PA excitation processes. We utilize this model to study the two-color 3D printing process, investigate the details of the evolutions of the reaction species as a function of time and space with varying laser power, and identify the dominant processes controlling the threshold power reduction of the fs laser.

2. Materials and methods

For two-color 3D printing, a typical custom-built two-photon lithography setup was modified to include a secondary laser path to the print plane. A simplified schematic of the setup is shown in Fig. 1(a). To induce TPA, we used an 80 MHz repetition rate, Ti:Sapphire fs oscillator (Coherent MIRA 900) with a center wavelength of 800 nm and a bandwidth of 8 nm. The pulse width measured through an autocorrelation measurement at the print plane was ~485 fs, while a ~388 nm beam waist was determined from a gold bead scan [40]. A custom-built dispersion pre-compensation setup comprised of a pair of highly dispersive ultrafast mirrors (Edmund Optics) was incorporated into the setup. A 532 nm nanosecond (ns) pulsed fiber laser (MPB Communications Inc.) with an 80 MHz repetition rate and 1.2 ns pulse width was used for 1PA. This ns pulsed beam was designed to spatially overlap with the fs laser beam at the print plane with a spot size approximately 1.25 times larger than the fs beam. Both laser pulses were transmitted through lens pairs to control the size and focal plane position. They were then focused through a glass substrate into the photoresist using a 100X oil immersion objective lens (Nikon, NA = 1.49). All the laser powers were measured at the back of the objective lens through a 6 mm diameter aperture to replicate the entrance pupil of the objective lens. Power at the print plane was calculated assuming 70% transmission through the objective lens. A helium-neon (HeNe) laser was introduced to the combined laser beam path for repeatable focus detection at the print plane.

To develop a photoresist system with a photoinitiator supporting two-color 3D printing, (2E,6E)-2,6-Bis (4-(dibutylamino)benzylidene)-4-methylcyclohexanone (BBK) was added to the monomer, pentaerythritol triacrylate (PETA, Sigma-Aldrich), at a loading of 0.7% (by weight) [20,41]. The sample photoresist volume required for printing was prepared by placing a drop of photoresist in a ~40 µm tall gap between a microscope slide and a coverslip. Lines and 3D structures were printed on the coverslip surface. A piezo-actuated tip/tilt mirror (Physik Instrumente) was used to scan the laser beam for both line and 3D structure printing. An Electro-Optic Modulator (EOM, Conoptics) was used for shutter control. To print 3D woodpiles, both beams remained stationary at the print plane, and a five-axis PZT actuated linear nano-positioning stage (Mad City Labs) was used to print the structure. After printing, the fabricated lines and 3D structures were first developed in an isopropanol bath for 20 minutes. Then, they were moved to a new bath for 2-3 minutes followed by drying with nitrogen. After development, the samples were sputter coated with ~30 nm of Au/Pd mixture and imaged with a scanning electron microscope (SEM, Hitachi S-4800). Linewidths were measured by processing the SEM images through a MATLAB edge-finding algorithm [39].

Optics EXPRESS

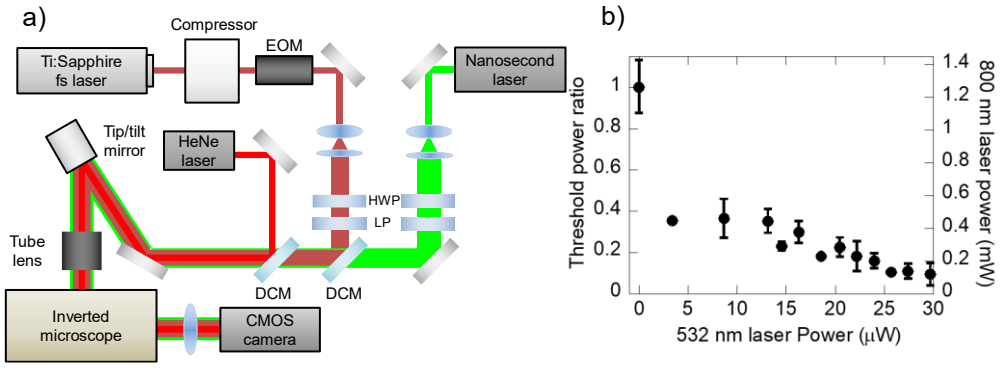

Fig. 1. (a) Simplified schematic of the two-color printing experimental setup. A half-wave plate (HWP) and linear polarizer (LP) combination are used for power control. Multiple beams are introduced into the same path using dichroic mirrors (DCM). (b) 800 nm fs laser threshold power reduction in two-color line printing. The threshold power ratio is defined as the ratio of the reduced fs laser threshold power for two-color printing to the fs laser only threshold power for single-color printing. The threshold power for line printing decreases as 532 nm laser power is increased. The error bars correspond to the standard deviation of the 800 nm laser power measurement for that data point.

3. Experimental results

3.1. Threshold power reduction in line printing

Reducing the threshold power of an 800 nm fs laser for TPP using the 1PA from a 532 nm laser was first verified with line printing experiments. We printed 30 μm long lines at 100 μm-s^{-1} speed using only the 800 nm fs laser. The fs laser only polymerization threshold for line printing is the minimum power required for yielding well-defined polymer lines. This power was determined by observing the lines after the development process using an Olympus BX40 microscope. Then, lines were printed using both the 800 nm fs laser and the 532 nm laser simultaneously. For every increment in 532 nm laser power, the fs laser power was reduced continuously until printed lines were no longer visible after development. This fs laser power denotes the new reduced threshold value for that fixed 532 nm laser power. In Fig. 1(b), the fs threshold power ratio is plotted against the 532 nm laser power used during two-beam printing. The threshold reduction ratio is defined as the ratio of the reduced fs laser threshold power for two-beam printing to the fs laser only threshold power for single-beam printing. The zero power of the 532 nm laser indicates printing with fs laser only where the threshold ratio is 1. The error bars in the plot are the standard deviation of threshold power values calculated from multiple experiments. The plot shows a significant reduction in fs laser power requirement well below 50% for line printing. The reduction in fs laser threshold power increases with the increase in 532 nm laser power. In two-beam printing, the addition of 532 nm laser power does not significantly increase the printed linewidth as TPA is still dominating the process. Using this setup, the minimum measured linewidth for single-beam printing is 221 nm whereas printing with two-beams at reduced threshold results in a 278 nm minimum linewidth. Beyond 30 μW 532 nm laser power, 1PA dominates the process and the 532 nm laser can print lines by itself. Although the initial linewidth with 1PA of 532 nm laser alone can be as low as 500 nm, while printing multiple lines accumulation effects take over and linewidths quickly rise to well beyond 1 μm.

Optics EXPRESS

3.2. Threshold power reduction in 3D printing

The threshold power was found to be different in the context of 3D printing as 3D structures printed at the gelation threshold of line printing cannot survive development as stable 3D parts. To compare threshold power reduction in 3D printing, woodpiles were chosen as model structures. $25 \times 25 \times 10\,\mu m$ woodpiles were printed at $100\,\mu m\ s^{-1}$ speed with the 800 nm fs laser only. When fs laser power was continuously reduced, the structures began collapsing below 1.6 mW. Hence, 1.6 mW fs laser power was taken as the threshold for single-beam stable 3D printing. This is higher than the 1.38 mW threshold power of line printing. Figure 2(a) shows the lowest power woodpile structure without collapsing. For printing woodpiles with two beams, a working range exists for 532 nm laser power. Using too little 532 nm laser power leads to no reduction in 3D printing threshold power. But if too much 532 nm laser power is used, single photon polymerization dominates the process, and the expected resolution cannot be maintained since reduction in photoinitiator concentration can cause large gradients in cross-linking density across the volume of the structure. Hence, we select a 532 nm laser power such that no 1PA induced accumulation or photoinitiator depletion occurs, and it only aids in reducing the threshold power while TPP from the 800 nm fs laser controls the resolution of the printing process. Considering all these factors, we were able to print woodpiles at roughly 50% fs laser power as shown in Fig. 2(b). The required threshold power for the fs laser is reduced more as the 532 nm laser power is increased. However, unlike line printing, threshold reduction below 50% cannot be achieved as the center of the structure starts to collapse due to photoinitiator depletion induced by 1PA.

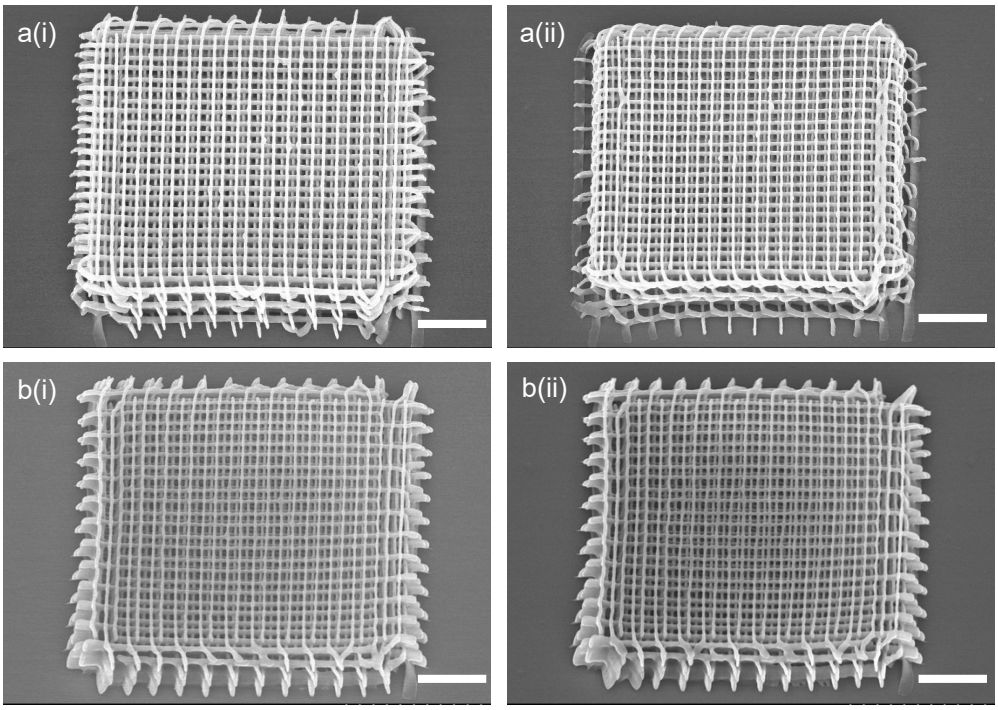

Fig. 2. Threshold power reduction in 3D printed woodpiles. Scale bar: 5 µm. (a) $25 \times 25 \times 10\,\mu m$ woodpiles printed at $100\,\mu m\ s^{-1}$ speed with 800 nm fs laser only. (i) 1.8 mW fs laser power, (ii) 1.6 mW fs laser power, threshold power for stable 3D printed structure. (b) woodpiles printed at ~50% fs laser power. (i) 0.92 mW fs laser power with 19.5 µW 532 nm laser power, (ii) 0.82 mW fs laser power with 23.4 µW 532 nm laser power.

Optics EXPRESS

Figure 3 shows the 3D printing of several other structures to demonstrate the capability of this process in reducing threshold power for printing arbitrary structures. The fs laser printing power required to print stable 3D structures can be reduced by as much as 50%. A higher degree of polymer conversion is usually needed for stable 3D structures. The range of 532 nm laser power (~18–24 μW) that can be used for printing arbitrary stable 3D structures at ~50% power, results in a ~80% reduction in line printing threshold power as seen in Fig. 1(b). Above this range, 1PA starts to dominate the two-color printing process. The hatching distance in these structures is increased to avoid 1PA induced photoinitiator depletion, resulting in rougher surfaces. The maximum height of the 3D structures is also limited by the photoinitiator depletion. Active power control of the 532 nm laser during printing or a better photoinitiator resupply method can help in extending the maximum height of fabricated structures.

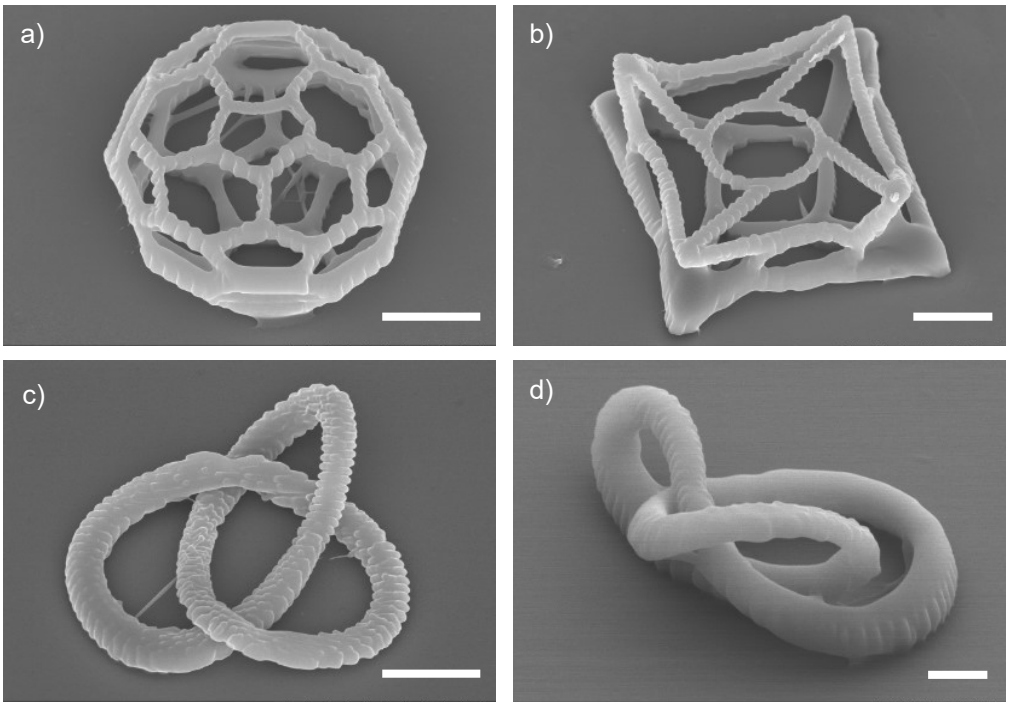

Fig. 3. 3D printed structures at ~50% fs laser threshold power. Scale bar: 5 μm. (a) Buckyball with 0.83 mW fs laser & 21.3 μW 532 nm laser power. (b) Chiral structure with 0.83 mW fs laser & 21.3 μW 532 nm laser power. (c) Trefoil knot like structure with 0.97 mW fs laser & 21.3 μW 532 nm laser power. (d) Trefoil knot like structure with 0.86 mW fs laser & 18.5 μW 532 nm laser power.

3.3. Effect of temporal synchronization

As both the 800 nm fs laser and the 532 nm ns laser have an 80 MHz repetition rate, they can be synchronized in time. To examine the effect of temporal alignment, four sets of woodpiles were printed (not shown here) at ~69% fs laser power and 5 μW ns laser power. The ns laser pulse was made to overlap with the fs laser pulse in time or come after it by 4 ns, 6.8 ns, and 11 ns respectively. All the results showed similar printed structures, indicating that the lifetime of the triplet state is long enough so that the effect of temporal alignment is negligible.

Optics EXPRESS

4. Photochemical process of threshold power reduction

4.1. Two-color printing process

The excitation of photoinitiator molecules followed by polymerization steps considered in this two-color printing process are illustrated in Fig. 4 along with the absorption spectra of the BBK photoinitiator and a simplified Jablonski diagram to represent our model. The absorption spectra at 0.38 mol% (0.7% by weight) in Fig. 4(a) indicate that there is a chance for both single-photon and two-photon absorption to occur. Even though a shorter wavelength light at ~450 nm will be more efficient for 1PA, we chose a longer wavelength 532 nm laser so that the printing process is not dominated by the 1PA process which has a poorer resolution. While the 800 nm fs laser induces simultaneous absorption of two photons from ground state S_0 to excited state S_1 through a virtual state, the 532 nm laser excites a single photon directly from the ground state to the excited state. In both cases, the molecule can relax back to the ground state through fluorescence (Fl) or to the Triplet state (T) going through inter-system crossing (ISC). From the triplet state, free radicals (R*) are generated, or the ground state is repopulated through phosphorescence (Ph). The radicals then react with free monomers (M) to create macroradicals (MR). These macroradicals then react with other free monomers to propagate the polymer chain and achieve higher cross-linking density. In the meantime, both radicals and macroradicals can be quenched by oxygen. Other termination mechanisms involve radical-radical or macroradical-macroradical or radical-macroradical reactions.

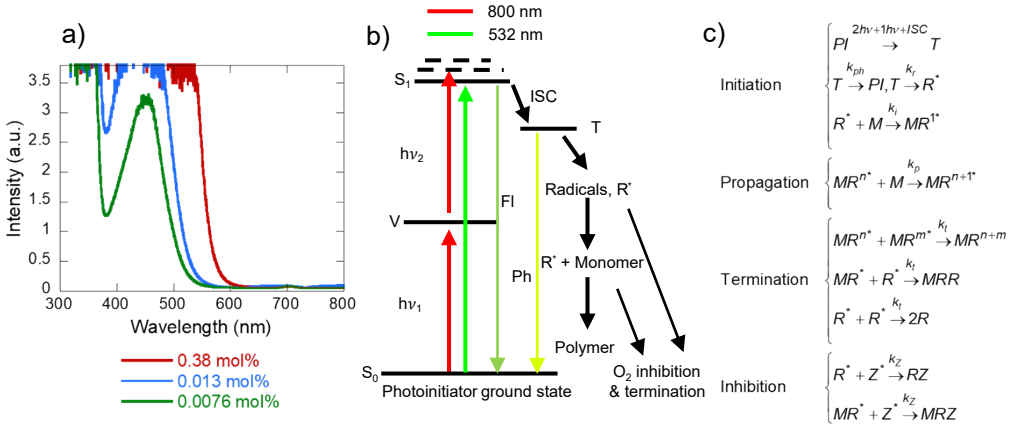

Fig. 4. (a) BBK photoinitiator absorption spectra for different concentrations. The peak absorption intensity values saturate the detector. (b) A simplified Jablonski for diagram two-color printing process. Both TPA and 1PA contribute to the population of the singlet state, then fluorescence (Fl) to the ground state or through intersystem crossing (ISC) to the triplet state. From the triplet state, phosphorescence (Ph), or radical generation occurs. Then radicals react with free monomers to initiate the polymer chain, or oxygen inhibition and termination. (c) The underlying polymerization steps are categorized into initiation, propagation, termination, and inhibition processes.

4.2. Mathematical model

The mathematical model is based on our previous work on the polymerization model for two-photon nanolithography [39]. The underlying chemical processes can be described through a set of spatiotemporal concentration rate equations involving six reaction species: ground-state photoinitiators [PI], triplet-state photoinitiators [T], radicals [R], free monomers [M], macroradicals [MR], and inhibitors (oxygen) [Z]. The effect of TPA by the 800 nm fs laser

Optics EXPRESS

and simultaneous 1PA by the 532 nm laser is described by the ground state and triplet state photoinitiator rate equations.

$$\frac{\partial[PI]}{\partial t} = d_{PI}\nabla^2[PI] - \phi_T\sigma_2\Phi^2[PI] - \varepsilon_g\frac{\Phi_g}{N_A}[PI] + k_{ph}[T] \tag{1}$$

$$\frac{\partial[T]}{\partial t} = \phi_T\sigma_2\Phi^2[PI] + \varepsilon_g\frac{\Phi_g}{N_A}[PI] - k_{ph}[T] - k_r[T] \tag{2}$$

The first term on the right-hand side of Eq. (1) indicates photoinitiator diffusion where d_{PI} is the photoinitiator diffusivity. The second and third term is the generation of triplet state photoinitiators due to TPA and 1PA respectively. For the 800 nm laser, ϕ_T represents the triplet quantum yield, σ_2 is the two-photon cross section, and Φ^2 indicates the photon flux for TPA where $\Phi = I(x, y, z, t)/h\upsilon$. For the 532 nm laser, ε_g is the molar extinction coefficient for 1PA, Φ_g is the photon flux, and N_A is Avogadro's number. The last term in Eq. (1) accounts for the relaxation from triplet state to ground state through phosphorescence where k_{ph} indicates the rate coefficient for this process. The triplet state photoinitiator rate equation involves one additional term for radical generation at a rate defined by coefficient k_r. From the triplet state, radical and macroradical generation, oxygen inhibition, and monomer conversion rate equations are the same for both TPA and 1PA.

$$\frac{\partial[R]}{\partial t} = k_r[T] - k_i[R][M] - k_t[R][MR] - 2k_t[R]^2 - k_Z[R][Z] \tag{3}$$

$$\frac{\partial[MR]}{\partial t} = k_i[R][M] - k_t[R][MR] - 2k_t[MR]^2 - k_Z[MR][Z] \tag{4}$$

$$\frac{\partial[Z]}{\partial t} = d_Z\nabla^2[Z] - k_Z[R][Z] - k_Z[MR][Z] \tag{5}$$

$$\frac{\partial[M]}{\partial t} = -k_i[R][M] - k_p[M][MR] \tag{6}$$

$$\frac{\partial C}{\partial t} = k_i[R][M] + k_p[M][MR] \tag{7}$$

Here, k_i, k_t, k_z, k_p represent kinetic rate coefficients for initiation, termination, inhibition, and propagation respectively. The diffusivity of oxygen is termed as d_z in Eq. (6) and C is the converted monomer concentration in Eq. (7).

Using the forward time centered space (FTCS) numerical method, these equations are solved in MATLAB. The model simulates the printing process of a 2 µm long line to ensure a steady printing process in a cross-section of 1000 nm x 1000 nm. In this work, we use a BBK photoinitiator and simulate the effect of printing with two beams for threshold reduction as compared to our previous work that uses an ITX photoinitiator for single-beam printing [39]. Hence, model parameters are divided into two parts where six impactful parameters unique to this work are varied to predict the experimental results accurately. The remaining parameters, including the ones that match our previous work, are held fixed. Table 1 lists these fixed parameters and their respective references. Five of the six fitting model parameters in Table 2 are determined by minimizing the error between experimental and simulated linewidths for printing with 800 nm fs laser only. The molar extinction coefficient for the 532 nm laser in Table 2 is determined by minimizing the error between experimental and simulated linewidths in two-color printing. As BBK is not a well-studied initiator, a range for the parameters was estimated using the parent molecule from which it was derived [41,42].

Optics EXPRESS

Table 1. Fixed model parameters

Parameter name	Symbol	Value	Reference
Laser wavelength		800 nm, 532 nm	Exp.
Repetition rate		80 MHz	Exp.
Pulse width (800 nm)		485 fs	Exp.
Pulse width (532 nm)		1.2 ns	Exp.
Beam waist		388 nm	Exp.
Free monomer initial concentration	$[M]_i$	3900 mol m^{-3}	Exp.
Photoinitiator initial concentration	$[PI]_i$	15 mol m^{-3}	Exp. estimation
Inhibitor initial concentration	$[Z]_i$	4.55 mol m^{-3}	[39,43]
Triplet quantum yield (800 nm)	ϕ_T	0.90	Estimation [42]
Kinetic rate coefficient for initiation	k_i	50 m^3 mol^{-1} s^{-1}	[44]
Kinetic rate coefficient for termination	k_t	1 m^3 mol^{-1} s^{-1}	[45]
Kinetic rate coefficient for inhibition	k_z	3.82×10^4 m^3 mol^{-1} s^{-1}	[32,39]
Inhibitor diffusivity	d_z	2.19×10^{-10} m^2 s^{-1}	[32,39]

Table 2. Fitting model parameters

Parameter name	Symbol	Value	Reference
Photoinitiator diffusivity	d_{PI}	7.14×10^{-11} m^2 s^{-1}	2.22×10^{-11} m^2 s^{-1} [39,46]
Molar extinction coefficient (532 nm)	ε_g	240 $M^{-1}cm^{-1}$	$<$ 800 $M^{-1}cm^{-1}$ (Exp. estimation)
Two-photon cross section (800 nm)	σ_2	19.18 GM	~191 GM [42]
Kinetic rate coefficient for propagation	k_p	9.4 m^3 mol^{-1} s^{-1}	2.08 m^3 mol^{-1} s^{-1} [39,45]
Kinetic rate coefficient for radical generation	k_r	1.27×10^6 s^{-1}	1.06×10^5 s^{-1} [47]
Kinetic rate coefficient for phosphorescence	k_{ph}	5.9×10^3 s^{-1}	5.9×10^5 s^{-1} [47]

4.3. Computational results and discussion

4.3.1. Comparison with experimental data

Using the model parameters described in Table 1 and Table 2, linewidth versus laser power and linewidth versus laser scanning speed results are compared against experimental data for both single-beam and two-beam printing in Fig. 5. The change in printed linewidth with fs laser power at 100 µm s^{-1} speed is shown in Fig. 5(a), and Fig. 5(b) shows the change in linewidth vs. laser scanning speed while keeping the 800 nm fs laser power constant at 1.87 mW. For each experimental data point in Fig. 5(a) and Fig. 5(b), 10 lines 60 µm long are printed 1 µm apart. The linewidths measured through image processing of SEM images are then averaged to get one data point. The error bars represent the standard deviation of the linewidths data averaged to get this one point. A minimum linewidth of 221 nm can be achieved while printing with the 800 nm fs laser (only) at 1.38 mW. Below this linewidth, printed lines did not remain sufficiently upright to be measured. Simulated linewidths are determined by finding the locations within which the degree of monomer conversion is above 25%. The trend in both plots shows good agreement between results obtained from simulation and experiment. Figure 5(c) shows the change in linewidth for two-beam printing where 800 nm laser power is held constant at 0.69 mW and 532 nm laser power is continuously increased. Each data point represents the linewidth measurement of one 30 µm long line at 100 µm s^{-1} speed as subsequent lines can be affected by the 532 nm laser power. The error bars represent the standard deviation of the linewidth measurement data taken from different parts of that one line. For two-beam printing,

Optics EXPRESS

the minimum measured linewidth is 278 nm for a combination of 0.69 mW 800 nm laser power and 5.86 µW 532 nm laser power. The computed linewidths trend in Fig. 5(c) shows a reasonable agreement with the experimental results. There exists a departure of data points at low 532 nm laser power since lines start to fall over at low laser power, and it becomes hard to measure the original linewidths after development.

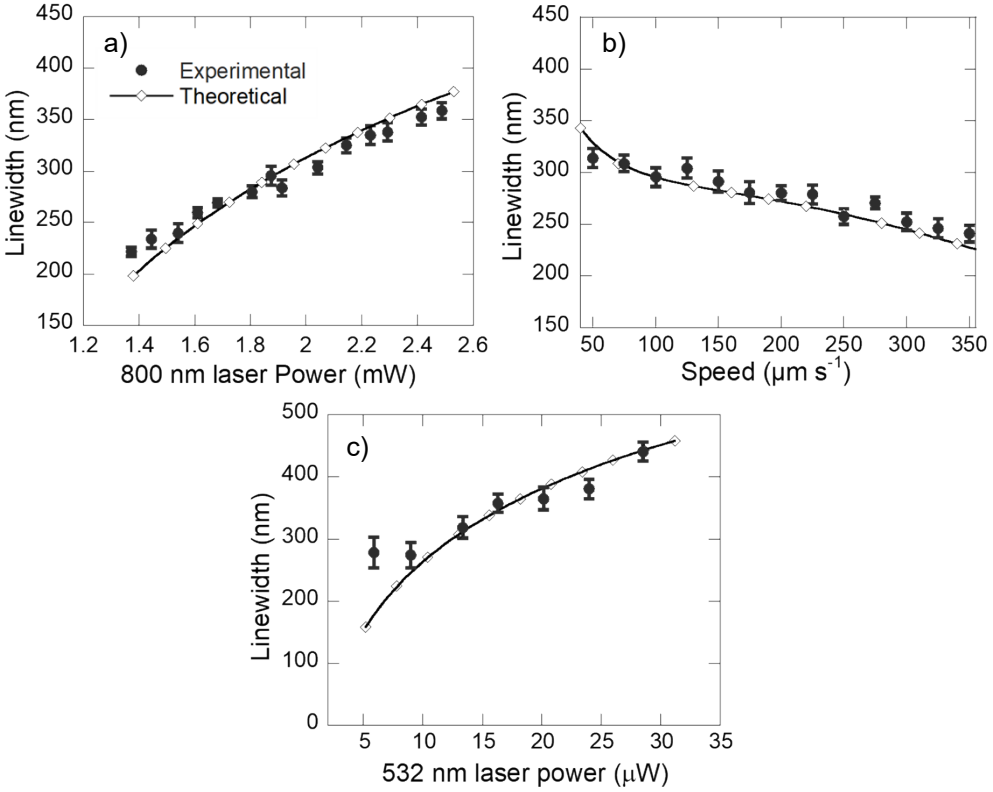

Fig. 5. (a) The experimental data of linewidth versus fs laser power compared with the results of the numerical simulation. (b) The experimental data of the linewidth versus fs laser scanning speed compared with the results of the numerical simulation at fs laser power of 1.87 mW. (c) Linewidth versus laser power comparison for two-color printing. The fs laser power is fixed at 0.69 mW and 532 nm laser power is gradually increased. The departure of experimental data at ~5 µW 532 nm laser power is due to lines falling over at low power after the development process. All the error bars correspond to the standard deviation of the linewidth measurement for that data point.

4.3.2. Contribution of reaction species for threshold power reduction

To understand the two-color printing process and determine the dominant processes controlling reduction in fs laser power, we investigate the temporal evolution of reaction species first. We compute the printing of a 2 µm long line at 100 µm s^{-1} speed. Temporal evolution data are taken at 1 µm from the starting location of the laser to ensure steady printing. Four sets of laser power combinations shown in Fig. 6 are selected to compare the cases of printing with fs laser only, 50% of fs laser power (only), a combination of fs laser and 532 nm laser, and 532 nm laser only. The 532 nm laser power is carefully selected to get similar linewidth in two-beam and single-beam (800 nm laser) printing for comparison purposes. From Fig. 6(a), it is seen that a similar degree of monomer conversion is possible at 50% fs laser power if we use a sufficient amount of 532 nm

Optics EXPRESS

laser power at the same time. At those power levels, the 532 nm laser or the 800 nm laser working alone cannot achieve sufficient monomer conversion to survive the development process.

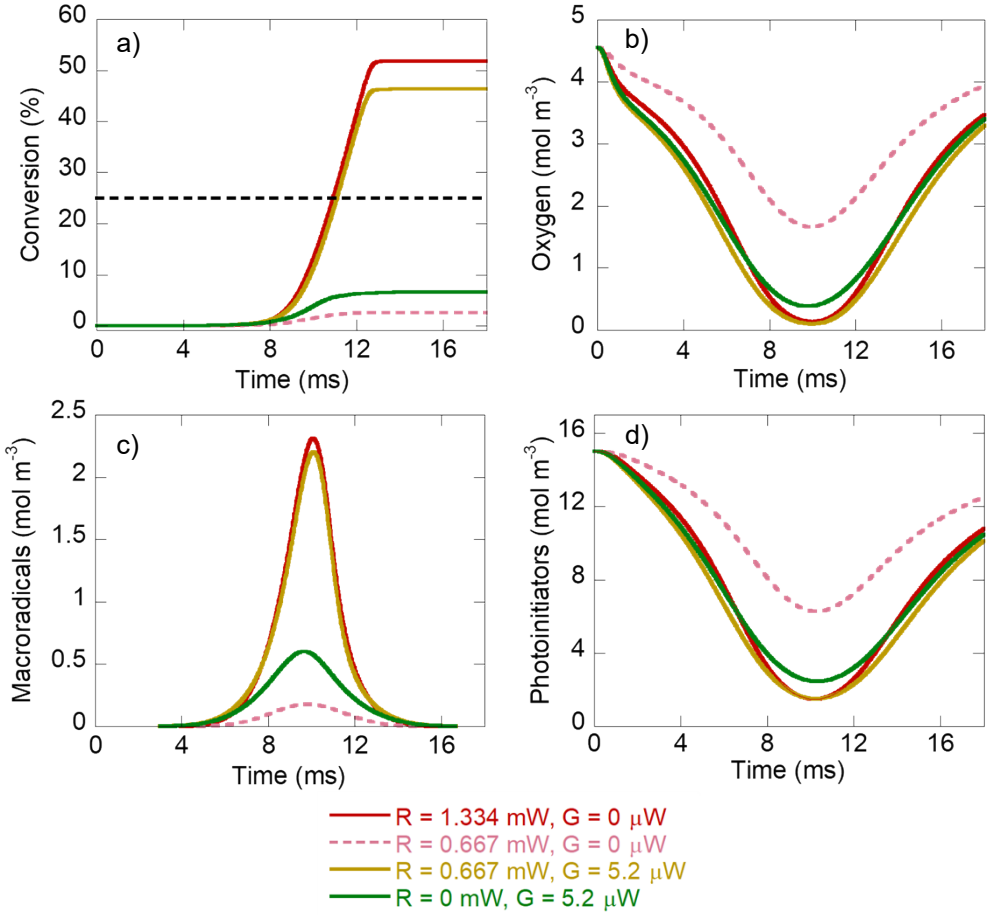

Fig. 6. Evolution of reaction species with time. Simulating the printing of a 2 μm long line at 100 μm s^{-1} speed, temporal development values of (a) monomer conversion, (b) oxygen concentration, (c) macroradical concentration, and (d) photoinitiator concentration are taken at 1 μm from the starting location of the laser. Four combinations of laser powers are used to show the effect of two-color printing in threshold power reduction.

Analysis of the evolution of species' concentrations suggests that oxygen quenching plays an important role in the polymerization process. The rate of oxygen diffusion from the surrounding area into the focal volume inhibits photoexcitation by TPA and 1PA [31,32]. At high enough fs laser power or in the case of two-color printing, oxygen is depleted below a certain level as shown in Fig. 6(b). A simultaneous increase in radical to macroradical conversion can be seen in Fig. 6(c). Note that the 532 nm laser (alone) is efficient at reducing the oxygen concentration as shown in Fig. 6(b) (the green line). When oxygen is close to depletion, radical to macroradical conversion increases rapidly. That is, the concentration of macroradicals in Fig. 6(c) would increase rapidly with the increase of the laser power. This also suggests that, when combined with 50% fs laser power, a careful selection of the 532 nm laser power is needed to avoid over-polymerization and simultaneous photoinitiator depletion as shown in Fig. 6(d).

To further understand the effects of both laser powers on the reaction species, we investigate the most developed state (maximum or minimum value) of the reaction species in the temporal

Optics EXPRESS

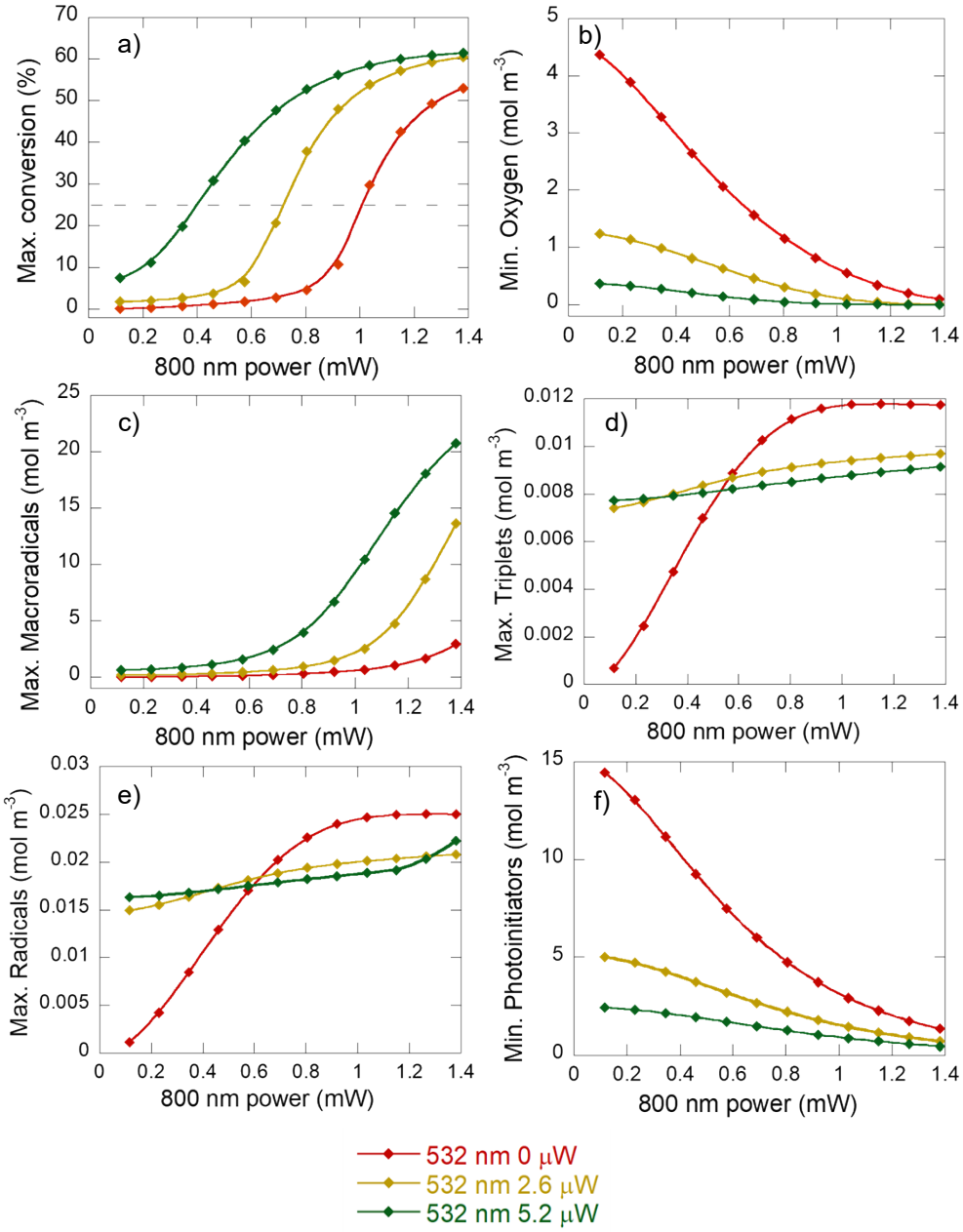

Fig. 7. Variations of reaction species with laser power. (a) monomer conversion, (b) oxygen concentration, (c) macroradical concentration, (d) triplet concentration, (e) radical concentration, and (f) photoinitiator concentration in their most developed state (maximum or minimum value) in the temporal domain are plotted as a function of laser powers.

domain as shown in Fig. 7. These values are also taken at 1 μm from the starting location of the laser to ensure steady printing. The maximum fs laser power in the bottom axes in Fig. 7 is the power at which the minimum experimental linewidth was measured. The three lines in each plot represent different amounts of 532 nm laser power, 0, 2.6 μW, and 5.2 μW which was

Optics EXPRESS

used in line printing. The maximum amount of monomer conversion vs. laser power is shown in Fig. 7(a). Conversion over 25% can be achieved at a fs laser power greater than 1 mW alone. In two-color printing, a similar amount of monomer conversion can be achieved at a much lower fs laser power with the increase of 532 nm laser power.

From Eq. (5) and temporal plots in Fig. 6, a reduction in oxygen concentration is necessary for radicals and macroradicals to continue the reactions to form the polymer chain. Figure 7(b) shows the minimum oxygen concentration achieved vs. fs laser power. The oxygen depletion level when fs laser prints alone is achieved at a lower fs laser power when two beams are printing simultaneously. A similar trend can be seen in the maximum macroradicals concentration generated in Fig. 7(c).

Figures 7(d) and Fig. 7(e) show the change in maximum number of triplets and radical concentration with laser power. They show a similar trend due to the direct dependence of radical generation on the triplet concentration as described in Eq. (2) and Eq. (3). Although the addition of 532 nm laser helps in increasing the radical generation, at high fs laser power alone, more radicals are generated compared to when the 532 nm laser is used. This is because apart from oxygen, the 532 nm laser also consumes photoinitiators more rapidly than the fs laser alone, as shown in Fig. 7(f). The reduction in photoinitiator in fact limits the maximum amount of 532 nm laser power that can be used in this two-beam printing process. This limiting effect of photoinitiator diffusion on polymerization has also been discussed in the literature [32]. The experimental results like those shown in Fig. 2(b) but at higher 532 nm laser powers, where the middle part of woodpiles starts to collapse, also suggest the contribution of photoinitiator depletion compared to the edges where photoinitiator molecules can be resupplied by diffusion from its surroundings.

5. Conclusion

The method of two-color 3D printing to reduce the fs laser printing power is shown experimentally and explained with a photochemical model. Experimental results show the ability of this method to reduce the printing power of the fs laser by up to 80 percent for 2D structures and up to ~50 percent for 3D structures. Thus, allowing the upscaling of printing speed for standard fs laser-based systems. The addition of a 532 nm laser helps in reducing the oxygen concentration below a certain level required for the rapid increase in macroradical generation and subsequent monomer conversion. As TPP dominates the printing process, the typical TPP minimum feature size can be achieved for a certain range of combinations of fs and 532 nm laser power. Although the amount of threshold reduction increases with the 532 nm laser power, the simultaneous decrease in photoinitiator concentration limits the reduction of the fs threshold laser power to ~50 percent.

Funding. National Science Foundation (CMMI-2135585, DGE-1842166).

Acknowledgments. The authors would like to thank the U.S. National Science Foundation for its support under the grant CMMI-2135585. Jason Johnson acknowledges the U.S. National Science Foundation for support under the Graduate Research Fellowship Program (GRFP) under grant number DGE-1842166. We acknowledge Paul Somers for helpful discussions, Mauricio Segovia for help in building the setup, and Zihao Liang and Prof. B.W. Boudouris for the BBK absorption spectra.

Disclosures. The authors declare no conflicts of interest.

Data availability. Data underlying the results presented in this paper are not publicly available at this time but may be obtained from the authors upon reasonable request.

References

1. S. Maruo, S. Kawata, and O. Nakamura, "Three-dimensional microfabrication with two-photon-absorbed photopolymerization," Opt. Lett. **22**(2), 132–134 (1997).
2. S. Kawata, H. B. Sun, T. Tanaka, *et al.*, "Finer features for functional microdevices," Nature **412**(6848), 697–698 (2001).

Optics EXPRESS

3. H. Wang, W. Zhang, D. Ladika, *et al.*, "Two-photon polymerization lithography for optics and photonics: fundamentals, materials, technologies, and applications," Adv. Funct. Mater. **33**(39), 2214211 (2023).
4. P. Somers, A. Münchinger, S. Maruo, *et al.*, "The physics of 3D printing with light," Nat. Rev. Phys. **6**(2), 99–113 (2023).
5. S. O'Halloran, A. Pandit, A. Heise, *et al.*, "Two-photon polymerization: fundamentals, materials, and chemical modification strategies," Adv. Sci. **10**(7), 1 (2023).
6. J. Fischer and M. Wegener, "Three-dimensional direct laser writing inspired by stimulated-emission-depletion microscopy [Invited]," Opt. Mater. Express **1**(4), 614 (2011).
7. R. Wollhofen, J. Katzmann, C. Hrelescu, *et al.*, "120 nm resolution and 55 nm structure size in STED-lithography," Opt. Express **21**(9), 10831 (2013).
8. N. Li, R. R. Gattass, E. Gershgoren, *et al.*, "Achieving 1/20 resolution by one-color initiation and deactivation of polymerization," Science **324**(5929), 910–913 (2009).
9. P. Somers, Z. Liang, T. Chi, *et al.*, "Photo-activated polymerization inhibition process in photoinitiator systems for high-throughput 3D nanoprinting," Nanophotonics **12**(8), 1571–1580 (2023).
10. Z. Gan, Y. Cao, R. A. Evans, *et al.*, "Three-dimensional deep sub-diffraction optical beam lithography with 9 nm feature size," Nat. Commun. **4**(1), 2061 (2013).
11. N. Liaros and J. T. Fourkas, "Ten years of two-color photolithography [Invited]," Opt. Mater. Express **9**(7), 3006 (2019).
12. B. Harke, W. Dallari, G. Grancini, *et al.*, "Polymerization inhibition by triplet state absorption for nanoscale lithography," Adv. Mater. **25**(6), 904–909 (2013).
13. J. Fischer, J. B. Mueller, A. S. Quick, *et al.*, "Exploring the mechanisms in sted-enhanced direct laser writing," Adv. Opt. Mater. **3**(2), 221–232 (2015).
14. T. Chi, P. Somers, D. A. Wilcox, *et al.*, "Tailored thioxanthone-based photoinitiators for two-photon-controllable polymerization and nanolithographic printing," J. Polym. Sci., Part B: Polym. Phys. **57**(21), 1462–1475 (2019).
15. T. Chi, P. Somers, D. A. Wilcox, *et al.*, "Substituted thioxanthone-based photoinitiators for efficient two-photon direct laser writing polymerization with two-color resolution," ACS Appl. Polym. Mater. **3**(3), 1426–1435 (2021).
16. C. Ding, X. Liu, Q. Liu, *et al.*, "Subdiffraction 3D nanolithography by two-photon two-step absorption and photoinhibition," Laser Photon Rev **18**(3), 2300645 (2024).
17. P. Kiefer, V. Hahn, S. Kalt, *et al.*, "A multi-photon (7×7)-focus 3D laser printer based on a 3D-printed diffractive optical element and a 3D-printed multi-lens array," Light: Advanced Manufacturing **4**(1), 1–14 (2024).
18. B. Jiao, F. Chen, Y. Liu, *et al.*, "Acousto-optic scanning spatial-switching multiphoton lithography," Int. J. Extrem. Manuf. **5**(3), 035008 (2023).
19. S. K. Saha, D. Wang, V. H. Nguyen, *et al.*, "Scalable submicrometer additive manufacturing," Science **366**(6461), 105–109 (2019).
20. P. Somers, Z. Liang, J. E. Johnson, *et al.*, "Rapid, continuous projection multi-photon 3D printing enabled by spatiotemporal focusing of femtosecond pulses," Light: Sci. Appl. **10**(1), 199 (2021).
21. W. Ouyang, X. Xu, W. Lu, *et al.*, "Ultrafast 3D nanofabrication via digital holography," Nat. Commun. **14**(1), 1716 (2023).
22. L. Zhang, C. Wang, C. Zhang, *et al.*, "High-throughput two-photon 3D printing enabled by holographic multi-foci high-speed scanning," Nano Lett. **24**(8), 2671–2679 (2024).
23. D. Gonzalez-Hernandez, S. Varapnickas, A. Bertoncini, *et al.*, "Micro-optics 3D printed via multi-photon laser lithography," Adv. Opt. Mater. **11**(1), 2201701 (2023).
24. X. Porte, N. U. Dinc, J. Moughames, *et al.*, "Direct $(3+1)$D laser writing of graded-index optical elements," Optica **8**(10), 1281 (2021).
25. G. Von Freymann, A. Ledermann, M. Thiel, *et al.*, "Three-dimensional nanostructures for photonics," Adv. Funct. Mater. **20**(7), 1038–1052 (2010).
26. C. Maibohm, O. F. Silvestre, J. Borme, *et al.*, "Multi-beam two-photon polymerization for fast large area 3D periodic structure fabrication for bioapplications," Sci. Rep. **10**(1), 8740 (2020).
27. T. Frenzel, V. Hahn, P. Ziemke, *et al.*, "Large characteristic lengths in 3D chiral elastic metamaterials," Commun. Mater. **2**(1), 4–9 (2021).
28. V. Hahn, T. Messer, N. M. Bojanowski, *et al.*, "Two-step absorption instead of two-photon absorption in 3D nanoprinting," Nat. Photonics **15**(12), 932–938 (2021).
29. D. K. Limberg, J. H. Kang, and R. C. Hayward, "Triplet-triplet annihilation photopolymerization for high-resolution 3D printing," J. Am. Chem. Soc. **144**(12), 5226–5232 (2022).
30. S. N. Sanders, T. H. Schloemer, M. K. Gangishetty, *et al.*, "Triplet fusion upconversion nanocapsules for volumetric 3D printing," Nature **604**(7906), 474–478 (2022).
31. J. B. Mueller, J. Fischer, F. Mayer, *et al.*, "Polymerization kinetics in three-dimensional direct laser writing," Adv. Mater. **26**(38), 6566–6571 (2014).
32. L. Yang, A. Münchinger, M. Kadic, *et al.*, "On the Schwarzschild effect in 3D two-photon laser lithography," Adv. Opt. Mater. **7**(22), 1901040 (2019).
33. R. Pingali and S. K. Saha, "Reaction-diffusion modeling of photopolymerization during femtosecond projection two-photon lithography," Journal of Manufacturing Science and Engineering, Transactions of the ASME **144**(2), 1 (2022).

Optics EXPRESS

34. M. G. Guney and G. K. Fedder, "Estimation of line dimensions in 3D direct laser writing lithography," J. Micromech. Microeng. **26**(10), 105011 (2016).
35. N. Uppal, "Modeling of temperature-dependent diffusion and polymerization kinetics and their effects on two-photon polymerization dynamics," Journal of Micro/Nanolithography, MEMS, and MOEMS **7**(4), 043002 (2008).
36. A. Pikulin and N. Bityurin, "Spatial resolution in polymerization of sample features at nanoscale," Phys. Rev. B **75**(19), 195430 (2007).
37. R. Pingali, H. Kim, and S. K. Saha, "A computational evaluation of minimum feature size in projection two-photon lithography for rapid Sub-100 nm additive manufacturing," Micromachines **15**(1), 158 (2024).
38. N. Liaros, S. A. Gutierrez Razo, M. D. Thum, *et al.*, "Elucidating complex triplet-state dynamics in the model system isopropylthioxanthone," iScience **25**(1), 103600 (2022).
39. J. E. Johnson, Y. Chen, and X. Xu, "Model for polymerization and self-deactivation in two-photon nanolithography," Opt. Express **30**(15), 26824 (2022).
40. J. Fischer, G. Von Freymann, and M. Wegener, "The materials challenge in diffraction-unlimited dired-laser-writing optical lithography," Adv. Mater. **22**(32), 3578–3582 (2010).
41. P. Kiefer, V. Hahn, M. Nardi, *et al.*, "Sensitive photoresists for rapid multiphoton 3D laser micro- and nanoprinting," Adv. Opt. Mater. **8**(19), 2000895 (2020).
42. Z. Li, N. Pucher, K. Cicha, *et al.*, "A straightforward synthesis and structure-activity relationship of highly efficient initiators for two-photon polymerization," Macromolecules **46**(2), 352–361 (2013).
43. C. Decker and A. D. Jenkins, "Kinetic approach of O2 inhibition in ultraviolet and laser-induced polymerizations," Macromolecules **18**(6), 1241–1244 (1985).
44. M. R. Gleeson, S. Liu, J. Guo, *et al.*, "Non-local photo-polymerization kinetics including multiple termination mechanisms and dark reactions: Part III Primary radical generation and inhibition," J. Opt. Soc. Am. B **27**(9), 1804 (2010).
45. H. Duran, S. Meng, N. Kim, *et al.*, "Kinetics of photopolymerization-induced phase separation and morphology development in mixtures of a nematic liquid crystal and multifunctional acrylate," Polymer **49**(2), 534–545 (2008).
46. M. H. Schneider, Y. Tran, and P. Tabeling, "Benzophenone absorption and diffusion in poly(dimethylsiloxane) and its role in graft photo-polymerization for surface modification," Langmuir **27**(3), 1232–1240 (2011).
47. J. Christmann, X. Allonas, C. Ley, *et al.*, "Triazine-based type-II photoinitiating system for free radical photopolymerization: mechanism, efficiency, and modeling," Macromol. Chem. Phys. **218**(18), 1600597 (2017).